Multiomics reveals gut dysbiosis contributes to fatty acid dysmetabolism in early phase of acute myocardial infarction

Authors

Yong Fan[a], Jiajun Ying[a,b,c], Ning Huangfu[a,b,c], Kewan He[a,d], Teng Hu[a], Pengpeng Su[e], Xintao Hu[a], Hequn He[f], Wei Liang[g], Junsong Liu[b], Jinsong Cheng[b], Shiqi Wang[b], Ruochi Zhao[b], Hengyi Mao[b], Fuwei He[b], Jia Su[b], Honglin Zhou[b], Zhenwei Li[b], Xiaohong Fei[b], Xiafei Sun[b], Peipei Wang[b], Minfang Guan[b], Weiping Du[b], Shaoyi Lin[b], Yong Wang[b], Fangkun Yang[a], Renyuan Fang[b], Ziqing Kong[h], Xiaomin Chen[a,b,c *], Hanbin Cui[a,b,c *]

Yong Fan and Jiajun Ying contributed equally to this work.

Affiliations

[a] Key Laboratory of Precision Medicine for Atherosclerotic Diseases of Zhejiang Province, The First Affiliated Hospital of Ningbo University, Ningbo 315000, China.

[b] Cardiology Center, The First Affiliated Hospital of Ningbo University, Ningbo 315000, China.

[c] Ningbo Clinical Research Center for Cardiovascular Disease, Ningbo 315000, China.

[d] Present address: Department of Ultrasound, The Affiliated Hospital of Ningbo University, LiHuiLi Hospital, Ningbo 315040, China.

[e] Wenzhou Medical University, Wenzhou 325035, China.

[f] Department of Emergency, The First Affiliated Hospital of Ningbo University, Ningbo 315000, China.

[g] Clinical Laboratory, The First Affiliated Hospital of Ningbo University, Ningbo 315000, China.

[h] Calibra Lab in DI'AN Diagnostics, Key Laboratory of Digital Technology in Medical Diagnostics of Zhejiang Province, Hangzhou 310030, China.

* Corresponding author: X.C. (email: chxmin@hotmail.com) or H.C. (email: nbcui_nbdyyy@outlook.com)

Abstract

Background: Acute myocardial infarction (AMI) remains a major cause of death, with limited understanding of its early risk stratification. While late-stage AMI has recognized associations with gut microbiome disturbances, the connection to eAMI is less explored.

Methods: Using metabolomics and metagenomics, we analyzed 56 samples, comprising 30 eAMI patients (within 12 hours of onset) and 26 age- and gender-matched healthy controls, to discern the influence of gut microbes and their metabolites.

Results: We found the eAMI plasma is dominated by increased long-chain fatty acids (LCFAs), 14 of which provide differentiating power of eAMI patients from HCs. Multiomics analysis reveals up to 70% of the variance in LCFAs of eAMI patients can be explained by altered gut microbiome. Higher-resolution profiling of gut bacterial species demonstrated that bacterial structural variations are mechanistically linked to LCFAs dysregulation. By *in silico* molecular docking and *in vitro* thrombogenic assay in isolated human platelets, we highlighted that eAMI-associated LCFAs contribute to platelet aggregation, a driving factor for AMI initiation.

Conclusions: LCFAs hold significant potential as early biomarkers of AMI and gut microbiome contributes to altered LCFAs in eAMI. Further studies are imperative to expand upon these observations to better leverage LCFAs as a potential biomarker for eAMI and as a therapeutic target for inhibition of platelet aggregation in eAMI.

Introduction

Acute myocardial infarction (AMI), the most lethal type in coronary artery disease (CAD) and primary cause leading to human mortality and morbidity(1-3), is mainly resulted from the rupture or erosion of atherosclerotic plaque, accompanied by the formation of an occlusive or sub-occlusive thrombus in one or more coronary artery branches(4,5). Accordingly, AMI is divided into two subtypes, ST-segment elevation myocardial infarction (STEMI) and non-ST-segment elevation myocardial infarction (NSTEMI). It has been showed that systemic or local inflammation, imbalance in adaptive immune pathways can modulate atherosclerotic plaque activity and contribute to coronary dysfunction and myocardial ischemic necrosis(5-7). However, the exact underlying mechanism responsible for the progression of coronary artery disease and occurrence of adverse event remains unclear.

A rising body of epidemiological study suggests that gut microbiota have a pivotal role in low-grade inflammatory metabolic diseases such as obesity(8) and diabetes(9), which are considered risk factor for atherosclerotic development. Thereafter, pathological evidence indicates that bacteria from the gut or the oral cavity might translocate to and reside in atherosclerotic plaques and could affect the development of atherosclerotic cardiovascular disease (ASCVD)(10,11). Improved sequencing technology and bioinformatics analyses have provided the several significant associations between the microbiota taxa and ASCVD(12,13).

On how gut microbiota promote to the development of ASCVD, we have summarized recent advances in the atherosclerosis-linked alterations in gut microbiome, highlighting the microbiota-related circulating metabolites that accelerate the development of ASCVD(14). Microbiota-synthesized metabolites such as trimethylamine N-oxide, secondary bile acids, short-chain fatty acids, lipopolysaccharides and phenylacetylglutamine have been recognized as the important contributor to atherosclerotic consequences. Nevertheless, whether gut microbiota participate in the initiation of AMI, some observational study reported the statistical correlation between gut bacteria profiling and AMI clinical phenotype. However, results are inconsistent across previous findings(15,16).

So far, the reported investigations on the associations between intestinal microbes and AMI recruited mostly patients in the late or stable stage of AMI, sparse report on very early phase of disease has been shown. Whether gut microbes contribute to the early stage of AMI (eAMI) lesion through its derived metabolites remains unknown. Here, we recruited a cohort of 30 patients with eAMI within 12 hours and 26 normal controls, for whom we performed metagenomic sequencing of the gut microbiome and plasma metabolomics. We found that long-chain fatty acids (LCFAs) dominate the metabolome perturbations in eAMI plasma, and the gut microbiome at species level explains up to 70% of the variance in LCFAs composition in eAMI patients. We also found that eAMI-associated LCFAs may possess potent thrombogenic functionality by molecular docking and platelet aggregation assay, which furtherly supports the rational for causal relationship between altered gut microbiota and the initiation of AMI.

Materials and methods

Study design and cohort description

This study enrolled 30 AMI patients and 26 normal controls who were hospitalized in the First Affiliated Hospital of Ningbo University from February 2021 to November 2021. Participants were in strictly conformity with the inclusion and exclusion criteria (**Figure S1**). The diagnosis of AMI is based on the guidelines of the American Heart Association (ACC) in 2021(17).

Inclusion criteria were diagnoses of AMI defined as follows: cardiac troponin (cTn) I/T > the upper limit of the 99% normal reference value and have any one or more of the following: significant chest pain of myocardial ischemia; changes in newly diagnosed ischemic electrocardiogram (ST-T changes or left bundle branch block or pathological Q wave); imaging evidence suggested new loss of myocardial activity or regional wall motion abnormalities; abnormal coronary angiography.

Exclusion criteria were: history of digestive diseases; severe hepatic and renal dysfunction; history of autoimmune diseases, malignant hematological diseases and tumor; infection within one month of the study or the use of antibiotic or probiotic. Normal controls were hospitalized for health examination at the same period.

The study protocol was approved by the Ethics Committee of The First Affiliated Hospital of Ningbo University (No. 2021-R018-YJ01). The study was performed in accordance with the principles of the Declaration of Helsinki. All participants provided written, informed consent for participation in the study.

Sample collection and biochemical analysis

Peripheral venous blood was drawn immediately after the patients arrived at the emergency department, or first moments after hospitalization for normal control individuals. Blood samples were centrifuged immediately at 4 °C, 4000 rpm for 10 minutes, and the supernatant (plasma) was stored at −80 °C for further analysis. The first morning fresh fecal (each 400-600 mg) and urine samples were collected from all

the participants under the hospital diet, then placed into sterile cryotube and frozen at -80°C refrigerator before further use.

Whole blood samples for biochemical measurements were collected after at least 10-hour fasting period. The measurements of fasting glucose, lactate dehydrogenase, creatine kinase, c-reactive protein, serum alanine aminotransferase, aspartate aminotransferase, glutathione S-transferase, creatinine, glycated serum protein, high-density lipoprotein cholesterol, low-density lipoprotein cholesterol, apolipoproteins, lipoprotein, and serum amyloid A were performed by an autoanalyzer (AU5800, Beckmancoulter). HbA1C was measured by an automated clinical analyzer (H100plus, Lifotronic). Plasma brain natriuretic peptide level was measured by a full-automatic chemiluminescence immunoassay analyzer (Cobas e602, Roche). Plasma troponin was measured using an autoanalyzer (DXI800, Beckmancoulter). Urine samples were analyzed by urine sediment analyzer (UF-5000, Sysmex).

Pseudo-targeted metabolomics profiling and preprocessing

Metabolomic profiling was performed utilizing the CalOmics metabolomics platform at Calibra Lab, affiliated with DIAN Diagnostics. The analytical instrumentation comprised an ACQUITY 2D UPLC system (Waters, Milford, MA, USA) coupled with a Q Exactive (QE) hybrid Quadrupole-Orbitrap mass spectrometer (Thermo Fisher Scientific, San Jose, USA). Metabolites were analyzed, based on the chemical properties of the serum metabolites, utilizing both polar ionic and lipid modes.

Sample preparation involved the extraction of metabolites using a methanol solvent at a 1:4 ratio. Following extraction, mixtures were shaked for three minutes and subsequently subjected to centrifugation at 4000 × g for 10 minutes at 20°C to precipitate proteins. The resulting 100 µL aliquots of supernatant were transferred onto sample plates, dried under a stream of nitrogen, and reconstituted in appropriate solvents for injection into the UPLC-MS/MS system.

The QE mass spectrometer settings included a mass resolution of 35,000 and a scan range from 70 to 1000 m/z. For the first UPLC-MS/MS method, the instrument

operated in positive electrospray ionization (ESI) mode using a C18 reverse-phase UPLC column (UPLC BEH C18, 2.1x100 mm, 1.7 µm; Waters). The mobile phases consisted of water (A) and methanol (B) with 6.5 mM ammonium bicarbonate at pH 8 for gradient elution. The third method similarly employed the C18 reverse-phase column in ESI positive mode, but used a mobile phase of water (A) and a mixture of methanol, acetonitrile, and water (B) containing 0.05% perfluoropentanoic acid (PFPA) and 0.01% formic acid (FA). In the fourth method, the system was operated in negative ESI mode with a hydrophilic interaction liquid chromatography (HILIC) column (UPLC BEH Amide, 2.1x150 mm, 1.7 µm; Waters), and the mobile phases were water (A) and acetonitrile (B) containing 10 mM ammonium formate.

Following the preprocessing of raw data and rigorous data quality control assessments, ion peaks were extracted employing proprietary in-house information technology hardware and software systems. Metabolites were subsequently identified through querying a bespoke library, which was compiled using pure standards sourced from commercial providers or other available channels. The identification protocol for metabolites within the samples was stringent, requiring a precise match across three specific criteria when compared to the library entries: a narrow retention index window, mass accuracy within a 10 ppm deviation, and tandem mass spectrometry (MS/MS) spectra that exhibit high scores in both forward and reverse searches. Quantification of each metabolite was achieved by calculating the peak area using the area-under-the-curve (AUC) method. This approach ensures accurate measurement of metabolite concentrations within the samples.

Before statistical analysis, raw peak areas were normalized to adjust for system fluctuation among different run days. The normalized peak areas were then log-transformed (log2) to reduce data distribution skewness and be in approximate normal distribution (Gaussian distribution). Missing values in peak area matrix were imputed by using the minimal detection value of a metabolite among all tested samples.

DNA extraction and library construction of fecal samples

Deoxyribonucleic acid (DNA) was extracted from fecal samples utilizing the cetyltrimethylammonium bromide (CTAB) method. Control samples included unused swabs which were processed identically through the DNA extraction protocol to ensure absence of DNA amplification products. The resultant DNA was eluted in 50 µl of elution buffer, following a modified protocol provided by QIAGEN, and preserved at -80°C for subsequent analyses.

For polymerase chain reaction (PCR) analysis, the samples were processed at LC-BIO Technologies Co., Hangzhou, China. The construction of the DNA library was accomplished using the TruSeq Nano DNA LT Library Preparation Kit (FC-121-4001). Fragmentation of the DNA was performed using dsDNA Fragmentase (NEB, M0348S) at 37°C for 30 minutes. This step produced blunt-ended DNA fragments via a combination of fill-in reactions and exonuclease activity. Size selection was then conducted using the sample purification beads provided in the kit.

To prepare the DNA fragments for adapter ligation, an adenine (A) base was added to the blunt ends of each strand. Each adapter, designed with a thymine (T) base overhang, facilitates the ligation to the A-tailed DNA fragments. These adapters are crucial as they contain necessary sites for the hybridization of sequencing primers, enabling single, paired-end, and indexed sequencing reads.

Ligation involved either single or dual index adapters, and the products were subsequently amplified via PCR. The amplification parameters included an initial denaturation at 95°C for 3 minutes, followed by 8 cycles of denaturation at 98°C for 15 seconds, annealing at 60°C for 15 seconds, extension at 72°C for 30 seconds, and a final extension at 72°C for 5 minutes. This process prepares the library for high-throughput sequencing analyses.

Metagenomic sequencing data processing

Raw sequencing data were processed to generate clean reads suitable for downstream analyses. Initially, sequencing adapters were excised from the reads using Cutadapt (version 1.9). Subsequently, low-quality reads were trimmed using fqtrim (version 0.94), which employs a sliding-window algorithm. Reads were then

aligned to the host genome using Bowtie2 (version 2.2.0) to eliminate host-derived sequences. Following the quality filtering, the remaining reads were assembled de novo using IDBA-UD (version 1.1.1) to construct individual metagenomes for each sample. Predictions of coding regions (CDS) within the metagenomic contigs were performed by MetaGeneMark (version 3.26). The CDS sequences across all samples were clustered using CD-HIT (version 4.6.1) to generate a set of unigenes. Unigene abundance in each sample was estimated using transcripts per million (TPM) based on read alignment performed again with Bowtie2 (version 2.2.0). Taxonomic classification of the unigenes was achieved by aligning them to the NCBI non-redundant (NR) database using DIAMOND (version 0.9.14). The taxonomic annotations and abundance profiles of these unigenes were utilized to conduct differential analysis at both taxonomic and gene-specific levels. Enterotypes profiling was performed using pipeline as previously demonstrated (18). Phage-inclusive metagenomics profiling was conducted with Phanta.

Profiling of bacterial structural variations

Prior to the structural variations (SVs) classification, the iterative coverage-based read assignment pipeline was used to precisely reassign the ambiguous reads to the most likely reference(19,20). The reference genomes given in the proGenomes database (http://progenomes1.embl.de/) were concatenated, separated into genomic 1-kbp bins, and used for the detection of highly variable genomic variations. The SGV-Finder pipeline(19) was used to identify SVs that fall into one of three categories: (1) variable SVs, or vSVs, (2) deletion SVs, or dSVs; the presence or absence of a specific genomic segment was maintained; or (3) deletion SVs, or dSVs, with deletion percentages of >75% (this genomic segment was excluded from the analysis). All bacterial species with SV calling were found in at least 10% of all samples and were used in the analysis that followed.

Molecular docking simulation

The crystal structures of several human receptors were obtained from the RCSB Protein Data Bank (https://www.rcsb.org/). These include the free fatty acid receptor

1 (GPR40, PDB ID: 5TZY), the thromboxane A2 receptor (TXA2, PDB ID: 6IIV), and the P2Y purinoceptors 1 and 12 (PDB IDs: 4XNW and 7PP1, respectively). Subsequent to download, water molecules and co-crystallized ligands were removed from the .pdb files to prepare the proteins for molecular docking studies. For the docking simulations, the receptor structures were prepared by adding polar hydrogen atoms and computing partial charges using the Kollman and Gasteiger methods. These modifications were performed using AutoDock Tools (version 1.5.638). The prepared structures of both ligands and receptors were then saved in .pdbqt format, facilitating their use in subsequent molecular docking procedures. The molecular docking studies were performed using the open-source software AutoDock Vina (version 1.1.2) (21) investigate the interactions between AMI-associated long-chain fatty acids (LCFAs) and selected receptors involved in platelet aggregation. Adjustments to the grid box allowed the AutoDock algorithm to predict ligand conformations within the receptor binding sites and evaluate them using scoring functions (22), with the grid spacing set at 1 Å. The three-dimensional interactions between the selected receptors and long-chain fatty acids (LCFAs) were analyzed and visualized using the PyMOL Molecular Graphics System (version 2.5.0), an open-source platform. Subsequently, AutoDock version 4.2 was employed to predict the binding affinities between various ligands and the selected receptors, providing quantitative insights into the potential binding interactions (23).

Thrombogenic effect of LCFAs on isolated human platelets

Fresh platelets were obtained from normal human volunteers without any antiplatelet or anticoagulant drugs being used within 2 weeks. Whole blood was collected from the peripheral vein of healthy volunteers into 0.1 vol of ACD buffer (75 mM sodium citrate, 39 mM citric acid, and 135 mM dextrose, pH 6.5). Diluted whole blood was centrifuged at 1500g for 20 minutes at 25 ^{o}C, and platelet-rich plasma (PRP) was collected into a fresh tube. Then we diluted PRP in ACD buffer, and centrifuged it at 800g for 10 minutes at 25℃. The platelet pellet was then resuspended in Tyrode's buffer (137 mM NaCl, 2 mM KCl, 0.34 mM Na_2HPO_4, 12 mM

$NaHCO_3$, 1 mM $MgCl_2$, 5.5 mM glucose, 5 mM HEPES, and 0.35% BSA, pH 6.5) at 10^9 platelets/mL, and kept at 23 °C for up to 4 h before use.

Incubations of washed human platelets with fatty acids were done either in pH 6.5 phosphate buffer or in "pH 7.4 Tris buffer" (15.4 mM Tris-Cl, pH 7.4; 140 mM NaCl, 5.6 mM glucose(24)). Candidate LCFAs to be tested were chosen according to the results shown in **Figure 2a**. Then individual LCFA was diluted to specific concentration (1 mM, 2.5mM, 5mM and 10mM) by bovine serum albumin solution (BSA), respectively. Platelet aggregations were measured using a lumi-aggregometer (AG800, Shandong, China) at 37 ^{o}C under stirring at 1200 rpm.

Statistical analysis

In this study, no data were excluded before the statistical analysis. As the study is observational, no allocation or randomization was used. This study includes all available samples (n = 56) of patients with AMI and healthy individuals. Although sample sizes were not predetermined using statistical methods, our sample sizes are comparable to those published earlier(25,26). The distribution of samples among metagenomics and metabolomics batches was random. During the data collecting phases of the metagenomic, biochemical, and metabolomics, researchers were blinded to the group allocation.

All statistical analyses were performed with R (version 4.2.3). Significantly differed metabolites or taxa between AMI and control groups were found by parametric (student's *t*-test) or non-parametric (Wilcox's rank test) statistical methods. Multivariate analysis approaches including principal component analysis (PCA), principal coordinate analysis (PCoA), and random forest (RF) were also conducted. Permutational multivariate ANOVA (PERMANOVA) was performed to determine the differences in structures of global microbiome and LCFAs between AMI patients and controls by using *vegan* (v2.6-4) package. The association analysis between omics features were performed by spearman correlation using *cor.test* base command. Least absolute shrinkage and selection operator (LASSO) regression model was built by using *glmnet* (v4.1-7) package. Unless otherwise stated, all p values were

corrected using the Benjamini-Hochberg method andz Padj < 0.05 was considered statistically significant.

Results

Plasma metabolome and gut microbiome from a deeply phenotyped eAMI cohort

We profiled plasma samples collected from 30 early acute myocardial infarction (eAMI) patients (within 12 hours in emergency) and 26 age- and gender-matched healthy controls (HC), using mass spectrometry. For these participants, we also characterized gut microbiota by performing shotgun metagenomic sequencing of fecal samples. In addition, as shown in **Table 1**, it is important to note that HC in this study had no obstructions in in any of their coronary arteries, which was validated by coronary angiography, in addition to having bioclinical characteristics that were within heathy thresholds. As expected, eAMI patients are distinct from HC with elevated troponin, pro-BNP, and creatine kinase (p values < 1.0e-03) despite matching for age, sex, BMI and T2D status. Also, eAMI patients display increased inflammatory markers including C-reactive protein, white blood cells, neutrophils, and lymphocytes (p values < 1.0e-03).

A pseudo-targeted metabolomics platform was used to profile 926 identified metabolites, as well as 26 partially characterized features (**Table S1**). Metabolites belonged to diverse biochemical classes, including lipids, amino acids, xenobiotics, nucleotides, and carbohydrates (**Figure S2a**). Most metabolites (877) were measured in over 50% of the cohort, and 555 metabolites were present in all samples (**Figure S2b**). All the samples were randomly injected and median of RSDs for the internal standards used in the quality control samples is 2.78%, demonstrating the high quality of metabolomics data.

Bacterial DNA was extracted from fecal samples, sequenced on the Illumina platform, and a total of 402 Gb 150-bp paired-end reads were generated, with an average of 47.70 ± 5.98 (s.d.) million reads per sample (**Table S2**). For each sample, a majority of

high-quality sequencing reads (69.03–97.24%) were *de novo* assembled into long contigs or scaffolds, which were used for gene prediction, taxonomic classification, and profiling of structural variations (SVs) in bacterial genomes.

LCFAs dominate the metabolome perturbations in eAMI plasma

Principal component analysis of the 952 measured compounds is used in **Figure 1a** to show the remarkable differences in the global plasma metabolome of eAMI patients compared to HC subjects and individual contrasted metabolites are shown in **Figure S3**. To characterize the dysregulated metabolic pathways in patients with eAMI, we performed KEGG pathway enrichment analysis of the differential metabolites and observed that biosynthesis of unsaturated fatty acids (FA) was the most significantly disrupted in eAMI patients (**Figure 1b**). Moreover, we found that across the eAMI and HC groups, the 32 LCFAs species (saturated, monounsaturated, and polyunsaturated) showed considerable inter-individual heterogeneity (**Figure 1c**). Plasma LCFAs composition also displayed a significant variation between the two groups (permutational multivariate analysis of variance (PERMANOVA), $p < 1.0e\text{-}03$; **Figure 1d**), with 28 upregulated LCFAs between patients with eAMI and HC as demonstrated in the volcano plot (**Figure 1e**).

Thereafter, we divided our cohort into a training group (comprising 70% of the subjects) and a test set (comprising 30% of the subjects) to identify diagnostic biomarkers for differentiating HC and patients with eAMI. The training dataset was utilized to perform feature selection using LCFAs in plasma, and the selected features were then used to create a random forests classifier (**Figure 2a**). With an area under the receiver operating characteristic curve (AUC) of 0.927 in the training set, the random forests model by a biomarker panel of 14 LCFAs (**Figure 2b**) allowed differentiation between HC and eAMI groups (**Figure 2c**). The created classifier was subsequently used in testing dataset to estimate independent performance of our model, which had an AUC of 1 (**Figure 2d**). Overall, these findings reveal the differences of LCFAs alteration is dominant in metabolome perturbations of patients with eAMI and demonstrate LCFAs may allow to discover more potent biomarkers, making the diagnosis of eAMI more accessible.

Alterations in gut microbiome is associated with the LCFA dysmetabolism in eAMI

We next explored the underlying factors that regulate LCFA metabolism by factor analysis, where we found age, sex, and body mass index could only account for up to 10% of the variance in LCFA proportion (**Figure 3a**). This indicates that a large proportion of LCFA variation remains unexplained and may be attributed to other variables, for example, gut microbial factors. Consistent to previous reports(12), we identified that eAMI gut microbiome is not only distinct from but also more heterogenous than that of HC subjects (**Figure S4**). Furthermore, we found eAMI gut microbiome is marked by an enrichment in the Bacterides2 enterotype ($P_{\text{Fisher's exact test}}$ = 2.3e-02) with a slight depletion in Bacteroides1 enterotype ($P_{\text{Fisher's exact test}}$ = 3.1e-01, **Figure 3b**), which always represents a marker suggesting a high risk of metabolic disorders(27).

To furtherly understand if gut microbiome is involved in the regulation of LCFAs during the onset of eAMI, we performed a least absolute shrinkage and selection operator (LASSO) regression model to compute the variance in each of the detected LCFAs that can be explained by gut microbiome. Intriguingly, gut microbiome at species level explains up to 70% of the variance in LCFAs composition in this cohort (**Figure 3c**). We next sought to identify the potential bacterial taxa that associate with the LCFAs by spearman correlation. At genus level, *Mycobacteroides*, *Thermus*, and *Anaerostipes* are inversely linked to LCFAs (**Figure S5**). As shown in **Figure 3d**, we found *Streptococcus* species were negatively correlated with omega-3 polyunsaturated FAs including FFA 18:4 (n-3), FFA 18:3 (n-3 or -6), and FFA 22:5 (n-3), which were considered as cardioprotective compounds. Meanwhile, the *Streptococcus* species were found to be positively correlated with omega-6 polyunsaturated FAs and saturated LCFAs. Moreover, we discovered that the eAMI gut virome exhibits a decrease in *Vibrio* phage (**Figure 4a**) but enrichments in *Streptococcus* phage PH10 and *Streptococcus* phage SM1 (**Figure 4b**), both of which have known hosts that are *Streptococcus* species. *Streptococcus* bacterial species predominate in the eAMI gut microbiome (**Figure S4a**), although the mechanism underpinning this dominance is unclear. Nonetheless, the abundance in temperate lysogenic *Streptococcus* phages may provide some justification. Additionally, the total

number of virulent phages found in the eAMI gut microbiome is higher than in the healthy controls (Figure 4c). The ratio of virulent to temperate phages is also greater in the eAMI group compared to the HC group.

Gut bacterial structural variants profiling in eAMI

Structural variations (SVs) in bacterial genomes can disrupt gene function, thereby influencing the interactions between bacteria and their hosts (25). As a result, significant phenotypic and functional alterations within the gut microbiome of patients with early acute myocardial infarction (eAMI) may arise from differences in the presence or levels of SVs among genetically similar bacterial strains. Here, we profiled SVs in all samples and identified 4,234 deletion SVs and 1,948 variable SVs across 47 bacterial species (**Figures 5a** and **5b**). For some species, we observed considerable differences in copy number variation. We identified 87 deletion SVs and 18 variable SVs in *Bacteroides uniformis* across 134 individuals, 78 deletions and 15 variable SVs in *Faecalibacterium prausnitzii* in 124 individuals, and 110 deletion SVs and 55 variable SVs in *Parabacteroides distasonis* in 121 individuals. For the archaeal microbiota, we only identified SVs in *Methanobrevibacter smithii* in 13 individuals (**Figures 5a**). To explore potential differences in bacterial genetics, we further computed the Canberra distance of bacterial SV profiles between eAMI versus HC (**Figure 5c**). eAMI and HC samples were significantly different in the beta-diversity of SV composition (P_{Wilcoxon} = 1.4e-05) and composition of bacterial genetics in eAMI individuals has less heterogeneity than that of HC subjects.

Bacterial genetics associate to LCFAs dysmetabolism in eAMI

Exploring relationships between gut bacterial SVs and plasma LCFAs, we found that bacterial SVs were significantly related to LCFAs (**Figure 5d**). As a particularly notable example, in the association analysis between SVs in the *Alistipes shahii* genome and plasma LCFAs profile, we found that a 3-kbp deletion (*A. shahii*:575-578) was directly associated with FFA 22:4 and FFA 14:1 but inversely linked to FFA 16:0, indicating that this deletion SV may be involved in the regulation of LCFAs metabolism in eAMI (**Figure 5e**). According to gene analysis, the beginning of this specific genomic region

in *A. shahii* encodes a 3-oxoacyl-[acyl-carrier protein] reductase (*FabG*, **Figure 5f**), which is an enzyme catalyzes the NADPH-dependent reduction of beta-ketoacyl-ACP substrates to beta-hydroxyacyl-ACP products, the first reductive step in the elongation cycle of fatty acid biosynthesis. This deletion region is more prevalent in eAMI group compared to HC gut microbiome (**Figure 5g**). In accordance with the association analysis, we furtherly found that individuals with *A. shahii* genomes harboring this deletion have higher plasma FFA 22:4 and FFA 14:1 but lower level of FFA 16:0, compared to participants without this 3-kbp deletion in A. *shahii* genome (**Figure 5h**).

Molecular docking and thrombosis in human platelets support the thrombogenic effect of eAMI-associated LCFAs

We extended our work to *in silico* molecular docking to investigate the molecular connections that control thrombosis. Four canonical receptors that are involved in platelet aggregation—free fatty acid receptor 1 (GPR40), thromboxane A2 receptor (TXA2), P2Y purinoceptor 1 (P2Y1), and P2Y purinoceptor 12 (P2Y12)—were taken into account as binding receptors in the molecular docking models in addition to the 28 eAMI-associated LCFAs as binding ligands. As shown in **Figure 6a**, we selected the first-ranked complex models between the various LCFAs and these four receptors. Interestingly, the molecular docking models estimated substantial interactions between eAMI-associated LCFAs and four selected receptors, with binding affinity ranging from -5.7 to -9.1 kJ/mol (**Figure 5a**). Representative docking results for bindings between the chosen receptors and omega-3, -6, and -9 polyunsaturated FAs are displayed in **Figure 6b**.

Then, using *in vitro* human platelet anticoagulation assay, we aimed to experimentally validate the thrombogenic effects of eAMI-associated LCFAs. As shown in **Figure 6c**, we found omega-6 LCFAs significantly stimulate platelet aggregation at physiological concentrations (1 mM to 10 mM). As a non-ignorable example, FFA 19:1 (n-9), as a non-omega-6 LCFA, also causes strong thrombosis in human platelet (**Figure 6d**), while the mechanistic understanding behind this finding remains unknown. Our results imply suggest that eAMI-associated LCFAs may

446 possess potent thrombogenic functionality, making it fair to assume that they play a
447 significant role in host cardiometabolic health.

448 ## Discussion

449 The factors triggering the onset of AMI and the precise indicators of eAMI remain
450 unclear. However, the application of plasma metabolomics provides valuable insights
451 into the search for accurate diagnostic markers for complex conditions such as AMI.
452 Additionally, comprehensive multi-omics profiling plays a crucial role in unraveling
453 the underlying mechanisms responsible for AMI. Together, these approaches shed
454 light on both diagnostic advancements and a deeper dissection disentangling the
455 complexity of eAMI.

456 By plasma metabolomics profiling, we found that in patients with eAMI, there was a
457 remarkable increase in 28 LCFAs dominating the altered eAMI metabolome. These
458 LCFAs encompassed a variety of saturated, monounsaturated, and polyunsaturated
459 types. When investigating the etiology of LCFA dysmetabolism in eAMI, we initially
460 examined its correlation with conventional AMI risk factors including age, sex, body
461 mass index, and potentially diabetes. However, these factors alone could only explain
462 a maximum of 10% of the variation observed in LCFA proportions. This raises the
463 question of what accounts for the remaining 90% of LCFA variation. To this end, we
464 turned our attention to profiling the gut microbiota, as it is widely recognized for its
465 potential role in regulating the metabolome. The LASSO regression model allows us
466 to examine various factors influencing LCFA composition and reveals gut microbiome
467 at the species level accounted for up to 70% of the observed variance in the
468 composition of LCFAs. This finding suggests a significant association between the gut
469 microbiome and the alterations in LCFA levels.

470 To gain mechanistic insights behind the gut microbiome-LCFA interactions, we
471 associated bacterial SVs with LCFAs and observed significant relations. Of specific
472 interest is a 3-kbp deletion (*A. shahii*: 575-578) representing *FabG* gene, a key
473 enzyme in reduction step of elongation cycle in fatty acid biosynthesis, which is more
474 prevalent in eAMI gut microbiome, resulting in a relatively higher plasma FFA 22:4

and FFA 14:1 in eAMI patients. Others have already reported the increase of intracolonic saturated LCFAs positively associated with elevated abundances of *Prevotella, Lactobacillus*, and *Alistipes*(28). Additionally, the presence of *A. shahii* was also shown to strengthen the positive associations of red meat intake with trimethylamine N-oxide (TMAO) concentrations levels(29), while increased TMAO levels enhances platelet hyperreactivity and thrombosis risk(30), and is associated with an increased risk of incident major adverse cardiovascular events(31). These findings support that in addition to short-chain fatty acids – which are known gut microbial products – disturbances in the gut microbiota also contribute significantly to the variation in plasma LCFAs during eAMI.

Indeed, the question arises whether the elevated levels of LCFA in eAMI are merely a marker or if they hold pathophysiological significance. Considering that platelet activation is a distinct pathophysiological characteristic of eAMI, we sought to explore the impact of eAMI-associated LCFA on circulating platelet activation. As expected, we found a majority of omega-6 LCFAs rather than omega-3 LCFAs dose-dependently stimulate platelet aggregation. A role for omega-3 polyunsaturated fatty acids (PUFA) supplementation to achieve cardioprotective effects has also been shown by attenuating platelet function(32), aligning with our findings. To date, there is limited conclusive evidence regarding the effect of LCFAs on platelet activation, except for arachidonic acid (FFA 20:4 (n-6)), a well-known LCFA that activates platelets. However, our study has yielded intriguing results. We have discovered that both FFA 19:1 (n-9) (also known as 10-nonadecenoic acid, HMDB0013622) and FFA 22:4 (n-6) (Adrenic acid, HMDB0002226) can significantly induce human platelet aggregation to a similar degree as arachidonic acid (FFA 20:4 (n-6), see **Figure S6**). Notably, FFA 22:4 (n-6) can be synthesized from arachidonic acid (FFA 20:4 (n-6)), which, in turn, can be elongated from FFA 18:2 (n-6), also known as linoleic acid. These conversions and interactions among omega-6 PUFAs provide a potential mechanism for their role in activating platelets.

Consistent with previous reports(33), the outcome of our *in vitro* experiments supports many eAMI-associated LCFAs, especially omega-6 PUFAs can promote platelet aggregation even in normal physiological concentration (1-5 mM). However,

lots of epidemiological investigation has found higher intakes of omega-6 PUFA appear to be safe and may be even more beneficial, hence the AHA supports an omega-6 PUFA intake of at least 5% to 10% of energy for dietary recommendations of coronary heart disease(34). In another prospective analyses, higher *in vivo* circulating and tissue levels of LA and possibly AA were associated with lower risk of major cardiovascular events(35). Intriguingly, omega-6 PUFA, dihomo-γ-linolenic acid (FFA 20:3 (n-6)) has been shown to play a role in inhibiting platelet aggregation ex vivo, via COX-1–derived prostanoid metabolites(36). Therefore, it still has the overwhelming controversial data on potential effects of omega-6 PUFAs on platelet function.

While our study offered valuable multi-omics insights into a cohort of patients with eAMI, uncovering the association between gut dysbiosis and plasma metabolomic perturbations characterized by the notable enrichment of LCFAs, it is important to acknowledge certain limitations in our present study. Firstly, we propose that intestinal microbial disturbances are significantly associated with fatty acid dysmetabolism based on cross-sectional correlation analysis. However, the causal relationship between gut microbiota dysbiosis and altered FA metabolism remains unclear and requires confirmation in prospective cohorts. Secondly, while platelet activation is a characteristic feature of eAMI, the specific *in vivo* role of LCFAs is still not well understood, and there is ongoing debate regarding the effect of ω-6 LCFAs on platelet function. Thirdly, we still don’t know the direct or indirect effect of gut microbiota dysbiosis on platelet activation, as well the underlying mechanism responsible for it, despite there is report on TMAO(30) and phenylacetylglutamine(37) contributing to platelet hyperreactivity and enhanced thrombosis potential. Fourthly, although all participants followed a standardized in-hospital diet and stool samples were collected shortly after hospitalization, the potential influence of pre-hospital diet on intestinal microbiome and plasma metabolome profiling, as well as their interaction, cannot be completely ruled out. Finally, due to the limitations of sample size and the specific population background included in this study, the conclusions drawn from our findings should be furtherly validated through large-scale, prospective studies involving diverse regional populations.

Data availability

The metadata are available under restricted access due to participant consent and privacy regulations of this cohort, access can be obtained by request to the corresponding author. Access to the metagenomics and metabolomics data may be granted for statistical and scientific research with approval from the corresponding author (Hanbin Cui: hbcui_nbdyyy@outlook.com).

Code availability

Scripts associated with the data analysis and visualization are available at https://github.com/fjw536/AMI_gut_microbiome.

Acknowledgements

We thank the study participants and nurses for their contributions to the project. We gratefully acknowledge colleagues at Lianchuan biotechnology for Metagenomics sequencing analysis of gut microbiota, and DI'AN Diagnostics, Key Laboratory of Digital Technology in Medical Diagnostics of Zhejiang Province for plasma metabolomics profilling, data analysis and discussions.

Author contributions

Y.F., J.Y. and H.C. conceived and designed the study. J.Y., F.H., K.H., T.H., H.M., P.S. X.H., H.M., Z.L., R.Z., J.L., J.C., S.W., X.S., H.H., P.W., M.G., J.S., W.D., Y.W., H.Z., S.L., X.F., W.L., R.F., F.H. and X.C. were involved in the acquisition of samples and data. Y.F. and Z.K. analyzed and interpreted the data. Y.F. and J.Y. drafted the work and H.C. substantively revised it. All authors contributed to the article and approved the submitted version.

Competing interests

All authors declare no competing interests in this study.

Funding

562 This research was supported by the Key research and development project of
563 Zhejiang Province, China (no. 2021C03096), Major Project of Science and Technology
564 Innovation 2025 in Ningbo, China (no. 2021Z134) and Ningbo Clinical Research
565 Center for Cardiovascular Disease, Ningbo, China (no. 2022L001).

566

Reference

1. DALYs GBD, Collaborators H. Global, regional, and national disability-adjusted life years (DALYs) for 306 diseases and injuries and healthy life expectancy (HALE) for 188 countries, 1990-2013: quantifying the epidemiological transition. Lancet 2015;386:2145-91.
2. Faxen J, Jernberg T, Hollenberg J, Gadler F, Herlitz J, Szummer K. Incidence and Predictors of Out-of-Hospital Cardiac Arrest Within 90 Days After Myocardial Infarction. J Am Coll Cardiol 2020;76:2926-2936.
3. Gong W, Yan Y, Wang X et al. Risk Factors for In-Hospital Cardiac Arrest in Patients With ST-Segment Elevation Myocardial Infarction. J Am Coll Cardiol 2022;80:1788-1798.
4. Anderson JL, Morrow DA. Acute Myocardial Infarction. The New England journal of medicine 2017;376:2053-2064.
5. Crea F, Libby P. Acute Coronary Syndromes: The Way Forward From Mechanisms to Precision Treatment. Circulation 2017;136:1155-1166.
6. Maier W, Altwegg LA, Corti R et al. Inflammatory markers at the site of ruptured plaque in acute myocardial infarction: locally increased interleukin-6 and serum amyloid A but decreased C-reactive protein. Circulation 2005;111:1355-61.
7. Granger CB, Kochar A. Understanding and Targeting Inflammation in Acute Myocardial Infarction: An Elusive Goal. J Am Coll Cardiol 2018;72:199-201.
8. Turnbaugh PJ, Ley RE, Mahowald MA, Magrini V, Mardis ER, Gordon JI. An obesity-associated gut microbiome with increased capacity for energy harvest. Nature 2006;444:1027-31.
9. Karlsson FH, Tremaroli V, Nookaew I et al. Gut metagenome in European women with normal, impaired and diabetic glucose control. Nature 2013;498:99-103.
10. Jonsson AL, Backhed F. Role of gut microbiota in atherosclerosis. Nature reviews Cardiology 2017;14:79-87.
11. Barrington WT, Lusis AJ. Atherosclerosis: Association between the gut microbiome and atherosclerosis. Nature reviews Cardiology 2017;14:699-700.
12. Jie Z, Xia H, Zhong SL et al. The gut microbiome in atherosclerotic cardiovascular disease. Nature communications 2017;8:845.
13. Karlsson FH, Fak F, Nookaew I et al. Symptomatic atherosclerosis is associated with an altered gut metagenome. Nature communications 2012;3:1245.
14. Fan Y, Ying J, Ma H, Cui H. Microbiota-related metabolites fueling the understanding of ischemic heart disease. iMeta 2023;2:e94.
15. Kelly TN, Bazzano LA, Ajami NJ et al. Gut Microbiome Associates With Lifetime Cardiovascular Disease Risk Profile Among Bogalusa Heart Study Participants. Circulation research 2016;119:956-964.
16. Liu M, Wang M, Peng T et al. Gut-microbiome-based predictive model for ST-elevation myocardial infarction in young male patients. Frontiers in microbiology 2022;13:1031878.
17. Gulati M, Levy PD, Mukherjee D et al. 2021 AHA/ACC/ASE/CHEST/SAEM/SCCT/SCMR Guideline for the Evaluation and Diagnosis of Chest Pain: A Report of the American College of Cardiology/American Heart Association Joint Committee on Clinical Practice Guidelines. J Am Coll Cardiol 2021;78:e187-e285.
18. Vieira-Silva S, Falony G, Belda E et al. Statin therapy is associated with lower prevalence of gut microbiota dysbiosis. Nature 2020;581:310-315.

19. Zeevi D, Korem T, Godneva A et al. Structural variation in the gut microbiome associates with host health. Nature 2019;568:43-48.
20. Wang D, Doestzada M, Chen L et al. Characterization of gut microbial structural variations as determinants of human bile acid metabolism. Cell Host Microbe 2021;29.
21. Trott O, Olson AJ. AutoDock Vina: improving the speed and accuracy of docking with a new scoring function, efficient optimization, and multithreading. J Comput Chem 2010;31:455-461.
22. Pahonțu E, Proks M, Shova S et al. Synthesis, characterization, molecular docking studies and in vitro screening of new metal complexes with Schiff base as antimicrobial and antiproliferative agents. Appl Organometal Chem 2019;33:e5185.
23. Morris GM, Huey R, Lindstrom W et al. AutoDock4 and AutoDockTools4: Automated docking with selective receptor flexibility. J Comput Chem 2009;30:2785-2791.
24. Neufeld EJ, Wilson DB, Sprecher H, Majerus PW. High affinity esterification of eicosanoid precursor fatty acids by platelets. J Clin Invest 1983;72:214-220.
25. Fan Y, Støving RK, Berreira Ibraim S et al. The gut microbiota contributes to the pathogenesis of anorexia nervosa in humans and mice. Nat Microbiol 2023;8:787-802.
26. Kindschuh WF, Baldini F, Liu MC et al. Preterm birth is associated with xenobiotics and predicted by the vaginal metabolome. Nat Microbiol 2023;8:246-259.
27. Vieira-Silva S, Falony G, Belda E et al. Statin therapy is associated with lower prevalence of gut microbiota dysbiosis. Nature 2020;581:310-315.
28. Zhao L, Huang Y, Lu L et al. Saturated long-chain fatty acid-producing bacteria contribute to enhanced colonic motility in rats. Microbiome 2018;6:107.
29. Li J, Li Y, Ivey KL et al. Interplay between diet and gut microbiome, and circulating concentrations of trimethylamine N-oxide: findings from a longitudinal cohort of US men. Gut 2022;71:724-733.
30. Zhu W, Gregory JC, Org E et al. Gut Microbial Metabolite TMAO Enhances Platelet Hyperreactivity and Thrombosis Risk. Cell 2016;165:111-124.
31. Tang WH, Wang Z, Levison BS et al. Intestinal microbial metabolism of phosphatidylcholine and cardiovascular risk. The New England journal of medicine 2013;368:1575-84.
32. Adili R, Hawley M, Holinstat M. Regulation of platelet function and thrombosis by omega-3 and omega-6 polyunsaturated fatty acids. Prostaglandins Other Lipid Mediat 2018;139:10-18.
33. Schmitz G, Ecker J. The opposing effects of n-3 and n-6 fatty acids. Progress in lipid research 2008;47:147-55.
34. Harris WS, Mozaffarian D, Rimm E et al. Omega-6 fatty acids and risk for cardiovascular disease: a science advisory from the American Heart Association Nutrition Subcommittee of the Council on Nutrition, Physical Activity, and Metabolism; Council on Cardiovascular Nursing; and Council on Epidemiology and Prevention. Circulation 2009;119:902-7.
35. Marklund M, Wu JHY, Imamura F et al. Biomarkers of Dietary Omega-6 Fatty Acids and Incident Cardiovascular Disease and Mortality. Circulation 2019;139:2422-2436.
36. Yeung J, Tourdot BE, Adili R et al. 12(S)-HETrE, a 12-Lipoxygenase Oxylipin of Dihomo-gamma-Linolenic Acid, Inhibits Thrombosis via Galphas Signaling in Platelets. Arteriosclerosis, thrombosis, and vascular biology 2016;36:2068-77.
37. Nemet I, Saha PP, Gupta N et al. A Cardiovascular Disease-Linked Gut Microbial Metabolite Acts via Adrenergic Receptors. Cell 2020;180:862-877 e22.

Figure legends

Figure 1| Long-chain free fatty acids (LCFAs) dominate the metabolome alterations in plasma of early acute myocardial infarction (eAMI) patients compared with healthy control (HC) individuals. (a) Principal component (PC) analysis demonstrates the remarkable metabolome alterations in eAMI patients compared with HC individuals. **(b)** KEGG metabolic pathway enrichment of differential metabolites (FDR-adjusted $p < 0.05$) between eAMI and healthy controls. Fisher's exact test (one-side) followed by FDR-adjusted p value was used and only pathways with FDR-adjusted $p < 0.05$ were shown. **(c)** Proportional structure of 32 detected LCFAs in plasma across all samples of eAMI and HC individuals. LCFAs are colored by degree of saturation, saturated LCFAs are colored in yellow, monounsaturated LCFAs are colored in red, and polyunsaturated LCFAs are colored in blue. **(d)** Principal coordinate analysis (PCoA) plot of the difference between eAMI and HC groups based on LCFAs proportion profile. **(e)** Volcano plot of 952 detected metabolites by untargeted metabolome profiling in eAMI patients and HC individuals. Red dots represent significantly up-regulated (FDR-adjusted $p < 0.05$ and Cliff Delta > 0.4) metabolites in eAMI plasma. Blue dots represent notably eAMI-depleted plasma metabolites (FDR-adjusted $p < 0.05$ and Cliff Delta < 0.4). Grey dots marked the unchanged metabolites. Significantly altered LCFAs were labeled. The horizontal line represents FDR cutoff of 0.05 and the vertical lines denote $|\text{Cliff Delta}| > 0.4$.

Figure 2 | Machine learning demonstrates long-chain free fatty acids (LCFAs) are potential diagnostic biomarkers for eAMI. (a) The top 20 most important LCFAs reducing the variance (mean squared error (%IncMSE)) in classification of eAMI by random forest model. %IncMSE denotes the increase in mean squared error of predictions as a result of variable (LCFAs) being permuted. The training model was constructed by proportional profile of 32 LCFAs in 39 training samples. **(b)** Distribution of cross-validation error in random forest classification of eAMI patients as the number of top ranking LCFAs increased. Red dot line marks the optimal number of LCFAs ($n = 14$) for the classification of eAMI patients. **(c and d)** Receiver operating characteristic (ROC) curve using the 14 LCFAs optimized by random forest

model for the (**c**) training and (**d**) test set (right panel, *n* = 17). Vertical heatmap in each panel denotes specificity for the ROC curve in c and d. AUC, area under the curve.

Figure 3 | Bacterial alterations characterize eAMI gut microbiome and greatly explain the variance in plasma long-chain free fatty acids (LCFAs). **(a)** Density plot showing sample-wide distribution of (% of explained variances) intrinsic factors (gender, age, and body mass index (BMI)) associated with the plasma concentrations of LCFAs. **(b)** Bar plot demonstrates the variation of 32 LCFAs explained by identified bacterial taxa at species level using LASSO regression. **(c)** Stacked bar plot shows the prevalence of gut enterotypes in eAMI and control groups. **(d)** Circular heatmap represents the correlation between LCFAs and gut bacterial species. Only association groups with FDR-adjusted p value of < 0.01 are colored in this plot.

Figure 4 | Alterations in viral gut microbiota between eAMI and HC groups. Box plots showing the relative abundance of increased **(a)** and decreased **(b)** viral gut microbiota at species level in eAMI gut microbiome compared to that of HC group. Differences in abundance were detected using MaAslin2. **(c)** Significant variations in the abundance, abundance ratios, and counts of virulent and temperate phages between the HC and eAMI groups. Significance was determined by Wilcoxon ranked sum test. For box plots in all panels, the vertical lines extend 1.5 times the interquartile range (top and bottom borders of the box) and the median depicted by the horizontal line inside the box.

Figure 5 | Bacterial structural variations (SVs) links to long-chain free fatty acids profiles in acute myocardial infarction (AMI) patients. (a) Number of SVs of each bacterial species in 56 study participants. **(b)** Pie chart showing the total identified SVs numbers. **(c)** Boxplot of Canberra distance between samples within eAMI and healthy control (HC) groups based on SVs profile, significance is determined by two-sided Mann-Whitney *U*-test. **(d)** Chord diagram showing significant associations between LCFAs and bacterial SVs. **(e)** Heatmap demonstrates the associations between SVs of *Alistipes shahii* and LCFAs. Only significant correlations with FDR-adjusted p value of < 0.01 are visualized. ++, FDR-adjusted p < 0.01, and +++, FDR-

adjusted $p < 0.001$. **(f)** The deletion rate of the 3-kbp deletion harboring 3-oxoacyl-[acyl-carrier protein] reductase (FabG) in *Alistipes shahii*. **(g)** Stacking bar plot represents the prevalence of 3-kbp deletion SV of *Alistipes shahii* in eAMI and HC groups. **(h)** Relative abundance of LCFAs in individuals with and without the 3-kbp deletion SV of *Alistipes shahii*. **, $p < 0.01$, ***, $p < 0.001$ determined by two-sided Mann-Whitney *U*-test.

Figure 6 | Early acute myocardial infarction (eAMI)-associated long-chain free fatty acids (LCFAs) bind to thrombosis-related receptors and induce thrombosis in human platelets. (a) Heatmap of binding energies between eAMI-associated LCFAs and thrombosis-related receptors through molecular docking. Bing affinities are quantified at kJ/mol. **(b)** The representative AutoDock predicted binding conformation complex of LCFAs versus thrombosis-related receptors, within which the receptors are depicted as cartoons and LCFAs as sticks. **(c)** The thrombogenic impact of eAMI-associated LCFAs on human platelets is depicted in a heatmap. Platelet aggregation ratios of > 10% and 10% are indicated by blue and grey, respectively. **(d)** Representative platelet aggregation curves in a time interval of 300 seconds after the treatment of LCFAs at a concentration of 5 mM. Red dashed line indicates 10% threshold.

Supplementary Figures

Figure S1 | Participant flow diagram. 123 suspected myocardial infarction patients were contacted, and 30 were eventually enrolled after screening.

Figure S2 | a, Distribution of measured metabolite super pathways of the 952 metabolites. **b**, Distribution of metabolite prevalence among the 56 samples. Blue distribution represents prevalence of all analyzed metabolites ($n = 952$). Numbers of metabolites that are present in more than 50% ($n = 28$) of the samples are indicated by dashed lines.

Figure S3 | Metabolic alterations in the plasma of eAMI patients. Heatmap of

743 contrasted metabolites in the plasma of healthy controls (HC) and eAMI patients.

744 **Figure S4 | Alterations in bacterial gut microbiota in eAMI patients. a**, Phylogenetic
745 tree of contrasted bacterial taxa between eAMI and HC bacterial gut microbiota. Taxa
746 colored in red and blue respectively represents increased and reduced taxa in eAMI
747 bacterial gut microbiota compared with HC group. **b**. Box plot (line, median; box,
748 interquartile range (IQR); whiskers, 1.5× IQR) of β-diversity at bacterial species level
749 (Canberra distance) of eAMI (*n* = 30) and HC (*n* = 26) gut microbiota. Statistical
750 significances between two groups were determined by Wilcoxon rank-sum test (two-
751 sided).

752 **Figure S5 | Gut microbiome at genus level associate with long-chain fatty acids**
753 **(LCFAs) metabolism.** Circular heatmap represents the correlation between LCFAs and
754 gut bacteria at genus level. Association groups with FDR-adjusted p value of < 0.05
755 are visualized in this plot.

756 **Figure S6 | Thrombogenic effects of FFA 20:4 (arachidonic acid) in human platelets.**
757 Platelet aggregation curves in a time interval of 300 seconds after the treatment of
758 FFA 20:4 at concentrations of 500 μM and 1 mM are given in **(a)** and **(b)**, respectively.
759 Red dashed line indicates 10% threshold.

760

761 **Table 1. Cohort characteristics**

	eAMI, n = 30[1]	**Control**, n = 26[1]	**p-value**[2]
Sub-classification			
Control	0 (0%)	26 (100%)	
NSTEMI	5 (17%)	0 (0%)	
STEMI	25 (83%)	0 (0%)	
Gender			0.051
Female	3 (10%)	8 (31%)	
Male	27 (90%)	18 (69%)	
Age (ys)	56 (46, 66)	59 (43, 67)	>0.9
BMI （Kg/㎡）	26.4 (22.9, 28.3)	24.4 (22.0, 26.3)	0.2
Smoking (n)	19 (63%)	4 (15%)	<0.001
Alcohol (n)	10 (33%)	2 (7.7%)	0.020
Hypertention (n)	22 (73%)	9 (35%)	0.004
Diabetes (n)	7 (23%)	4 (15%)	0.5
Other commorbidities (n)	4 (13%)	4 (15%)	>0.9
Antithrombiotic (n)	1 (3.3%)	3 (12%)	0.3
Statin (n)	1 (3.3%)	2 (7.7%)	0.6
Antiarrhythmic (n)	2 (6.7%)	2 (7.7%)	>0.9
Antidiabetic (n)	4 (13%)	2 (7.7%)	0.7
Antihypertensive (n)	12 (40%)	8 (31%)	0.5
PPI (n)	1 (3.3%)	1 (3.8%)	>0.9
Culprit vessel (n)			
LM	1 (3.3%)	0 (0%)	>0.9
RCA	16 (53%)	0 (0%)	<0.001
LAD	22 (73%)	0 (0%)	<0.001
LCX	15 (50%)	0 (0%)	<0.001
Emergency troponin (ng/mL)	0 (0, 4)	0 (0, 0)	0.5
Emergency BNP (ng/L)	0.97 (0.13, 2.05)	0.98 (0.98, 0.98)	>0.9
In-hospital troponin (ng/mL)	37 (11, 99)	0 (0, 0)	<0.001
In-hospital Pro-BNP (ng/L)	395 (206, 1,039)	49 (17, 115)	<0.001
LDH (U/L)	0 (0, 473)	133 (133, 133)	0.7
Creatine kinase (U/L)	82 (40, 151)	2 (1, 3)	<0.001
CRP (mg/L)	0.9 (0.0, 3.6)	0.0 (0.0, 0.4)	0.003
WBC (*10^9/L)	12.4 (10.0, 13.3)	5.9 (4.9, 6.6)	<0.001
Neutrophils (%)	79 (73, 86)	57 (49, 65)	<0.001
Lymphocyte (%)	14 (9, 17)	33 (23, 39)	<0.001
Hemoglobin (g/L)	145 (135, 155)	138 (129, 156)	0.5
RDW (%)	12.50 (12.20, 12.78)	12.50 (12.20, 12.95)	0.7
ALT (U/L)	50 (36, 63)	17 (13, 28)	<0.001
AST (U/L)	252 (90, 358)	22 (18, 24)	<0.001
GST/GLT	3.82 (2.66, 5.49)	1.18 (0.88, 1.38)	<0.001
Creatinine (μmol/L)	73 (66, 88)	68 (55, 80)	0.068
BUN/creatinine	0.075 (0.053, 0.080)	0.070 (0.053, 0.090)	0.7
Uric acid (μmol/L)	361 (301, 513)	325 (252, 384)	0.035
Fasting glucose (mmol/L)	5.9 (5.3, 7.9)	4.9 (4.4, 5.2)	<0.001
HbA1C (%)	5.85 (5.53, 6.35)	5.40 (0.00, 5.77)	0.003
GSP (mmol/L)	1.89 (1.72, 2.19)	1.71 (0.35, 1.86)	0.009
Total cholesterol (mmol/L)	5.32 (4.44, 5.93)	4.24 (3.33, 5.18)	0.002
Triglycerides (mmol/L)	1.44 (0.95, 2.79)	1.19 (0.76, 1.53)	0.042
HDL (mmol/L)	1.01 (0.90, 1.10)	1.00 (0.86, 1.24)	0.9

	eAMI, n = 30[1]	**Control**, n = 26[1]	**p-value**[2]
LDL (mmol/L)	3.58 (2.92, 4.18)	2.81 (1.98, 3.16)	<0.001
apoB (g/L)	0.98 (0.82, 1.22)	0.59 (0.10, 0.79)	<0.001
apoA1 (g/L)	1.02 (0.90, 1.09)	1.02 (0.20, 1.22)	>0.9
LP(a) (mg/L)	14 (9, 25)	7 (0, 24)	0.063
SAA (mg/L)	15 (3, 32)	1 (0, 3)	<0.001
U-occult blood (n)			0.035
no	18 (60%)	20 (77%)	
Yes	12 (40%)	4 (15%)	
U-protein (n)			0.051
no	20 (67%)	21 (81%)	
Yes	10 (33%)	3 (12%)	
U-glucose (n)			0.037
no	23 (77%)	23 (88%)	
Yes	7 (23%)	1 (3.8%)	

[1]n (%); Median (IQR)

[2]Fisher's exact test; Pearson's Chi-squared test; Wilcoxon rank sum test

eAMI, early phase of acute myocardial infarction; NSTEMI, non-ST-elevation myocardial infarction; STEMI, ST-elevation myocardial infarction; BMI, body mass index; PPI, proton pump inhibitor; LM, left main; RCA, right coronary artery; LAD, left anterior descending artery; LCX, left circumflex artery; BNP, brain natriuretic peptide; CRP, C-reactive protein; WBC, white blood cell; RDW, red cell distribution width; ALT, alanine transaminase; AST, aspartate transaminase; GST/GLT, glutathione S-transferase; BUN, blood urea nitrogen; HbA1C, hemoglobin A1c; GSP, glycated serum protein; HDL, high-density lipoprotein cholesterol; LDL, low-density lipoprotein cholesterol; apo, apolipoprotein; LP, lipoprotein; SAA, serum amyloid A; U-, uric.

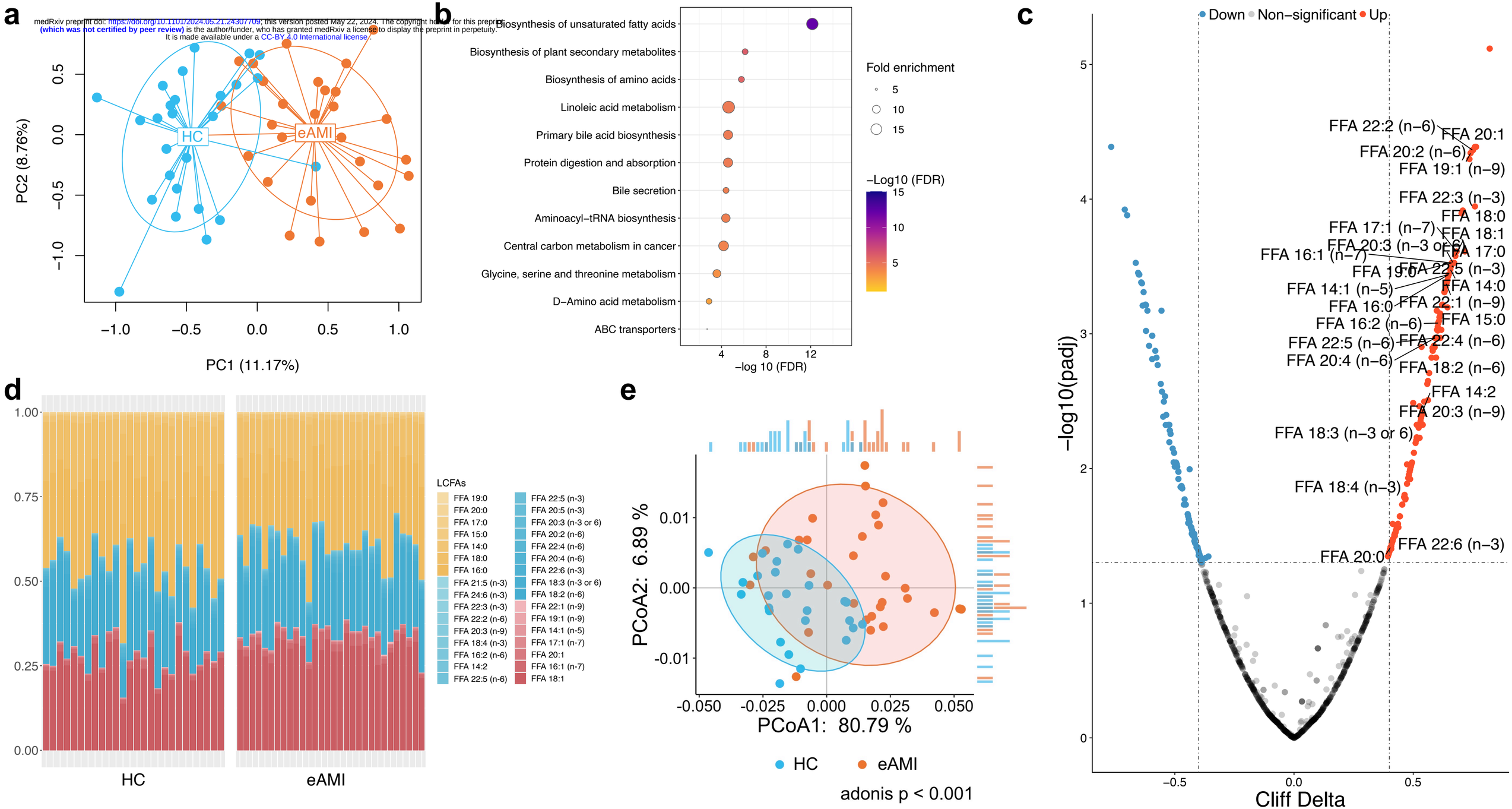

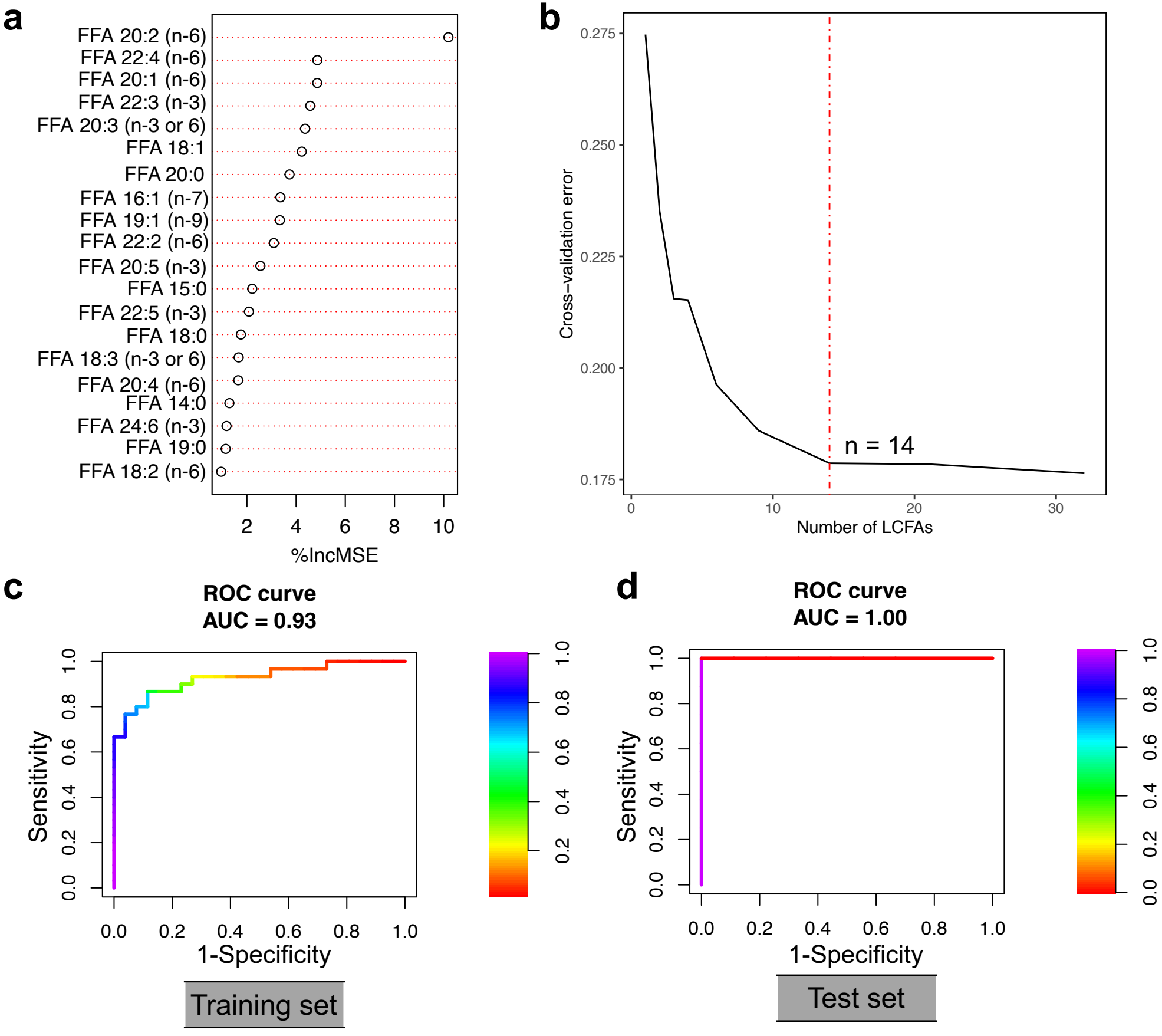
a
FFA 20:2 (n-6)
FFA 22:4 (n-6)
FFA 20:1 (n-6)
FFA 22:3 (n-3)
FFA 20:3 (n-3 or 6)
FFA 18:1
FFA 20:0
FFA 16:1 (n-7)
FFA 19:1 (n-9)
FFA 22:2 (n-6)
FFA 20:5 (n-3)
FFA 15:0
FFA 22:5 (n-3)
FFA 18:0
FFA 18:3 (n-3 or 6)
FFA 20:4 (n-6)
FFA 14:0
FFA 24:6 (n-3)
FFA 19:0
FFA 18:2 (n-6)
2 4 6 8 10
%IncMSE
b
Cross−validation error
0.275 0.250 0.225 0.200 0.175
n = 14
0 10 20 30
Number of LCFAs
c
ROC curve
AUC = 0.93
Sensitivity
0.0 0.2 0.4 0.6 0.8 1.0
1-Specificity
0.0 0.2 0.4 0.6 0.8 1.0
Training set
d
ROC curve
AUC = 1.00
Sensitivity
0.0 0.2 0.4 0.6 0.8 1.0
1-Specificity
0.0 0.2 0.4 0.6 0.8 1.0
Test set

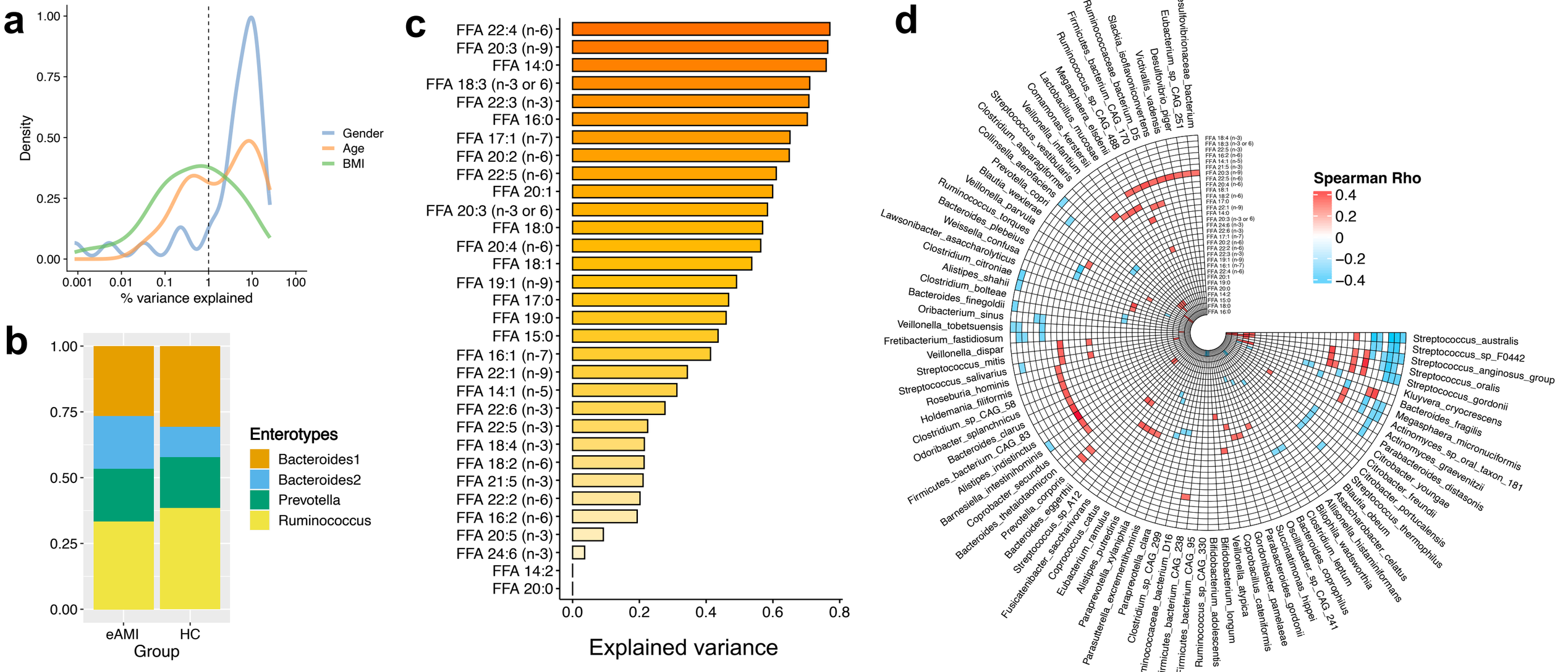
a
1.00
0.75
0.50
0.25
0.00
Density
0.001
0.01
0.1
1
10
100
% variance explained
Gender
Age
BMI
b
1.00
0.75
0.50
0.25
0.00
eAMI
HC
Group
Enterotypes
Bacteroides1
Bacteroides2
Prevotella
Ruminococcus
c
FFA 22:4 (n-6)
FFA 20:3 (n-9)
FFA 14:0
FFA 18:3 (n-3 or 6)
FFA 22:3 (n-3)
FFA 16:0
FFA 17:1 (n-7)
FFA 20:2 (n-6)
FFA 22:5 (n-6)
FFA 20:1
FFA 20:3 (n-3 or 6)
FFA 18:0
FFA 20:4 (n-6)
FFA 18:1
FFA 19:1 (n-9)
FFA 17:0
FFA 19:0
FFA 15:0
FFA 16:1 (n-7)
FFA 22:1 (n-9)
FFA 14:1 (n-5)
FFA 22:6 (n-3)
FFA 22:5 (n-3)
FFA 18:4 (n-3)
FFA 18:2 (n-6)
FFA 21:5 (n-3)
FFA 22:2 (n-6)
FFA 16:2 (n-6)
FFA 20:5 (n-3)
FFA 24:6 (n-3)
FFA 14:2
FFA 20:0
0.0
0.2
0.4
0.6
0.8
Explained variance
d
Desulfovibrionaceae_bacterium
Eubacterium_sp_CAG_251
Desulfovibrio_piger
Victivallis_vadensis
Slackia_isoflavoniconvertens
Ruminococcaceae_bacterium_D5
Ruminococcus_sp_CAG_488
Firmicutes_bacterium_CAG_170
Megasphaera_elsdenii
Ruminococcus_mucosae
Lactobacillus_kerstersii
Comamonas_antrihominis
Veillonella_infantium
Streptococcus_vestibularis
Clostridium_asparagiforme
Collinsella_aerofaciens
Prevotella_copri
Blautia_wexlerae
Veillonella_parvula
Ruminococcus_torques
Bacteroides_plebeius
Weissella_confusa
Lawsonibacter_asaccharolyticus
Clostridium_citroniae
Alistipes_shahii
Clostridium_bolteae
Bacteroides_finegoldii
Oribacterium_sinus
Veillonella_tobetsuensis
Fretibacterium_fastidiosum
Veillonella_dispar
Streptococcus_mitis
Streptococcus_salivarius
Roseburia_hominis
Holdemania_filiformis
Clostridium_sp_CAG_58
Odoribacter_splanchnicus
Bacteroides_clarus
Bacteroides_sp_CAG_83
Firmicutes_bacterium_CAG_83
Alistipes_indistinctus
Barnesiella_intestinihominis
Coprobacter_secundus
Bacteroides_thetaiotaomicron
Prevotella_corporis
Bacteroides_eggerthii
Streptococcus_sp_A12
Fusicatenibacter_saccharivorans
Coprococcus_catus
Eubacterium_ramulus
Alistipes_putredinis
Paraprevotella_xylaniphila
Parasutterella_excrementihominis
Paraprevotella_clara
Clostridium_sp_CAG_299
Ruminococcaceae_bacterium_D16
Firmicutes_bacterium_CAG_238
Firmicutes_bacterium_CAG_95
Ruminococcus_sp_CAG_330
Bifidobacterium_adolescentis
Bifidobacterium_longum
Veillonella_atypica
Coprobacillus_catenaformis
Gordonibacter_pamelaeae
Parabacteroides_gordonii
Sutterella_wadsworthensis
Oscillibacter_sp_CAG_241
Bacteroides_coprophilus
Clostridium_leptum
Bilophila_wadsworthia
Alistipes_finegoldii
Asaccharobacter_celatus
Blautia_obeum
Streptococcus_thermophilus
Citrobacter_freundii
Citrobacter_youngae
Parabacteroides_distasonis
Actinomyces_graevenitzii
Actinomyces_sp_oral_taxon_181
Megasphaera_micronuciformis
Bacteroides_fragilis
Kluyvera_cryocrescens
Streptococcus_gordonii
Streptococcus_anginosus_group
Streptococcus_oralis
Streptococcus_sp_F0442
Streptococcus_australis
FFA 18:4 (n-3)
FFA 18:3 (n-3 or 6)
FFA 22:5 (n-3)
FFA 16:2 (n-6)
FFA 14:1 (n-5)
FFA 21:5 (n-3)
FFA 20:3 (n-9)
FFA 22:5 (n-6)
FFA 20:4 (n-6)
FFA 18:1
FFA 18:2 (n-6)
FFA 17:0
FFA 22:1 (n-9)
FFA 14:0
FFA 20:3 (n-3 or 6)
FFA 24:6 (n-3)
FFA 22:6 (n-3)
FFA 17:1 (n-7)
FFA 20:2 (n-6)
FFA 22:2 (n-6)
FFA 22:3 (n-3)
FFA 19:1 (n-9)
FFA 16:1 (n-7)
FFA 22:4 (n-6)
FFA 20:1
FFA 19:0
FFA 20:0
FFA 14:2
FFA 15:0
FFA 18:0
FFA 16:0
Spearman Rho
0.4
0.2
0
−0.2
−0.4

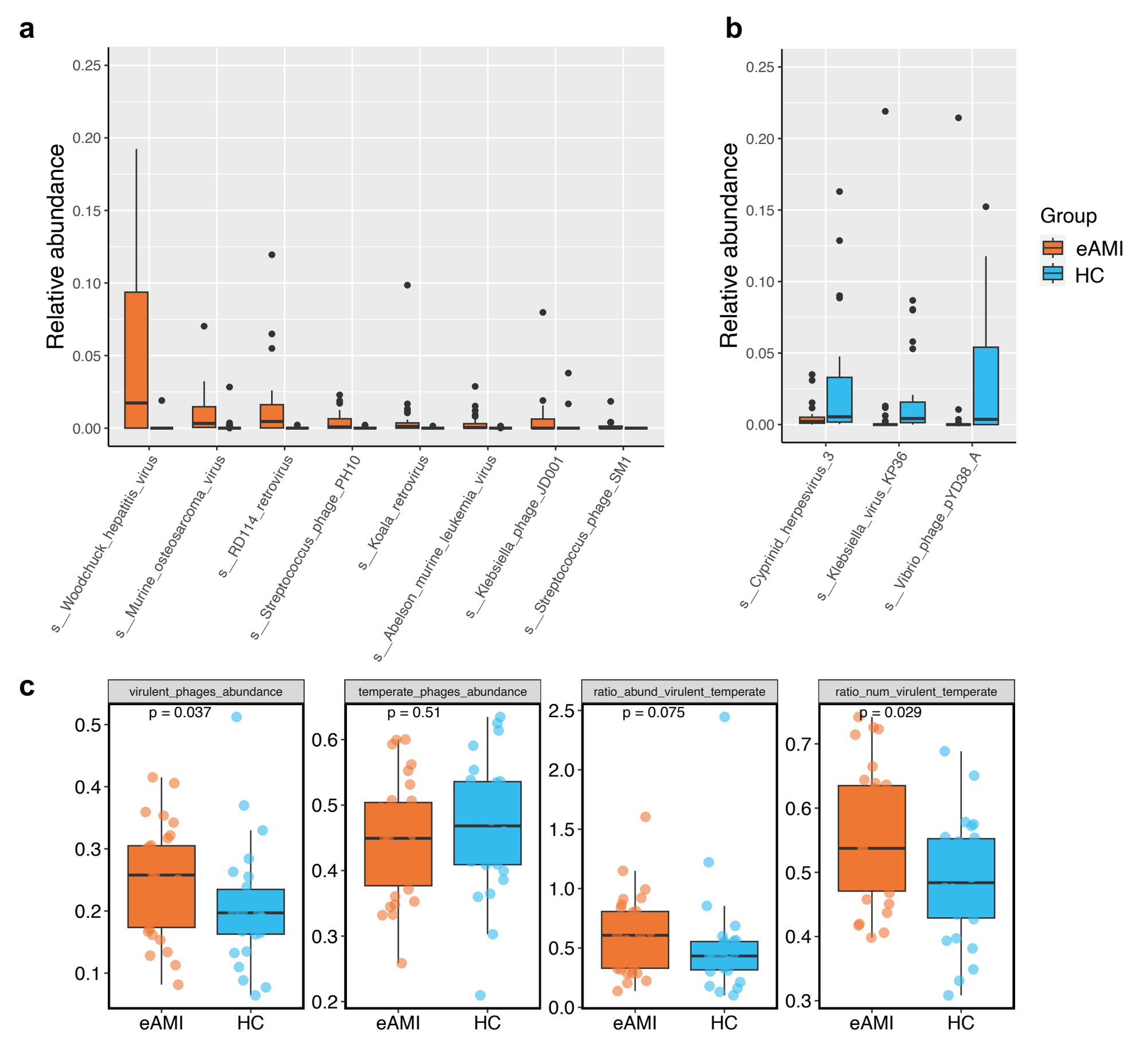
a
b
c
Relative abundance
0.25
0.20
0.15
0.10
0.05
0.00
s__Woodchuck_hepatitis_virus
s__Murine_osteosarcoma_virus
s__RD114_retrovirus
s__Streptococcus_phage_PH10
s__Koala_retrovirus
s__Abelson_murine_leukemia_virus
s__Klebsiella_phage_JD001
s__Streptococcus_phage_SM1
s__Cyprinid_herpesvirus_3
s__Klebsiella_virus_KP36
s__Vibrio_phage_pYD38_A
Group
eAMI
HC
virulent_phages_abundance
p = 0.037
temperate_phages_abundance
p = 0.51
ratio_abund_virulent_temperate
p = 0.075
ratio_num_virulent_temperate
p = 0.029
eAMI
HC

a

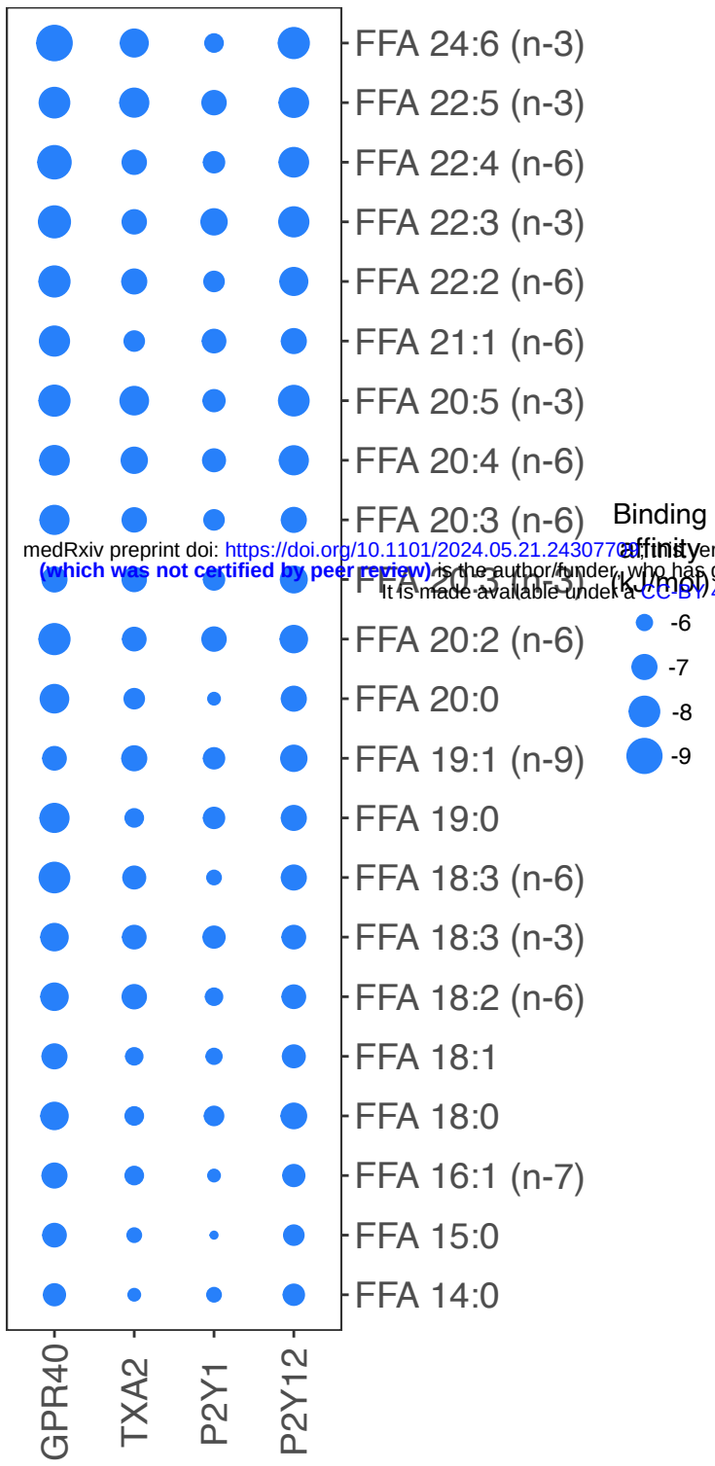

b

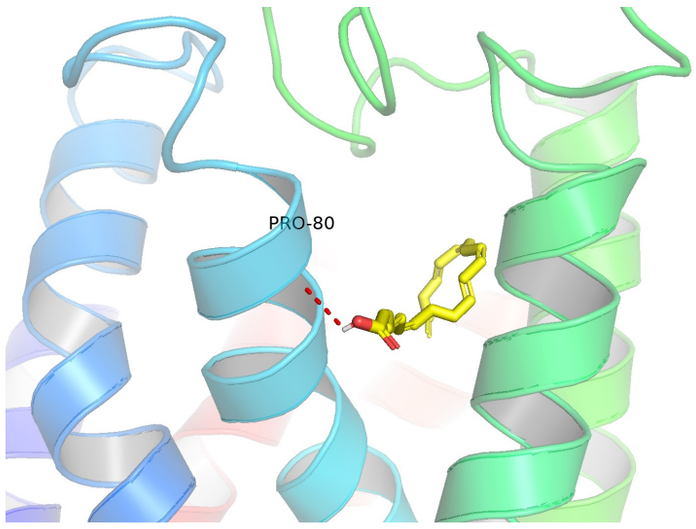

FFA 24:6 (n-3) + GPR40
(-9.1 kJ/mol)

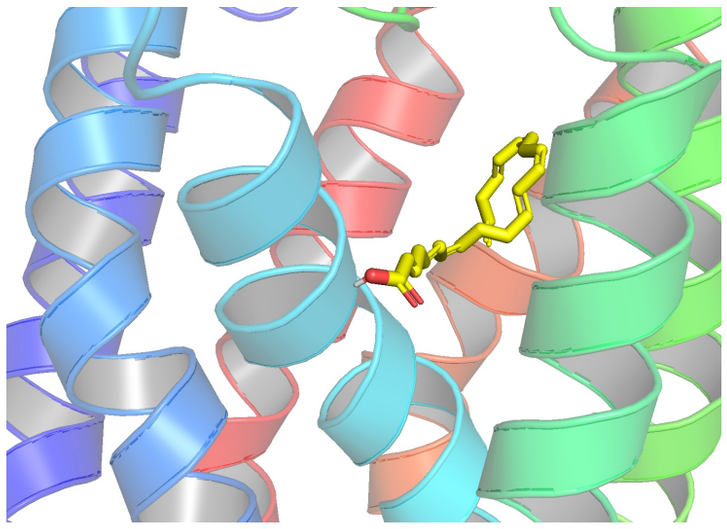

FFA 22:4 (n-6) + GPR40
(-8.6 kJ/mol)

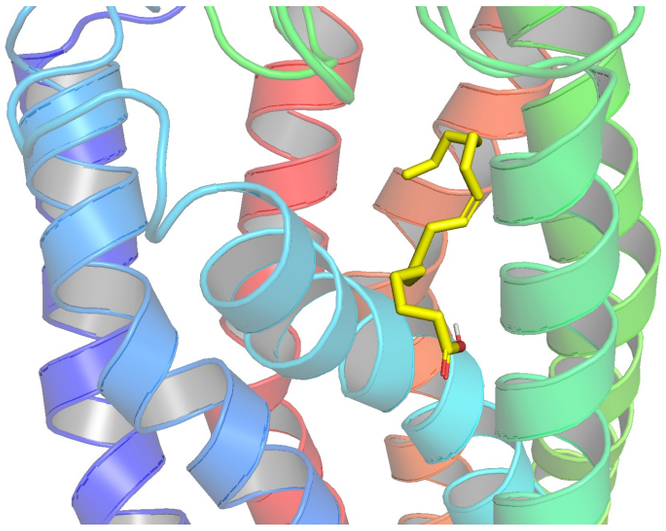

FFA 16:1 (n-7) + P2Y1
(-6.6 kJ/mol)

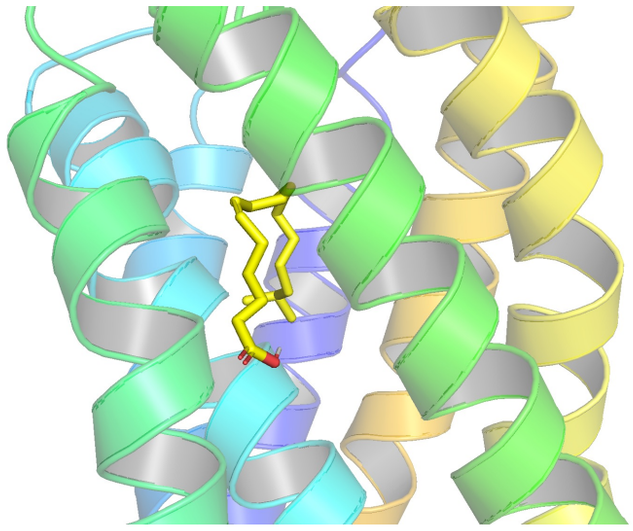

FFA 19:1 (n-9)+ P2Y12
(-7.2 kJ/mol)

c

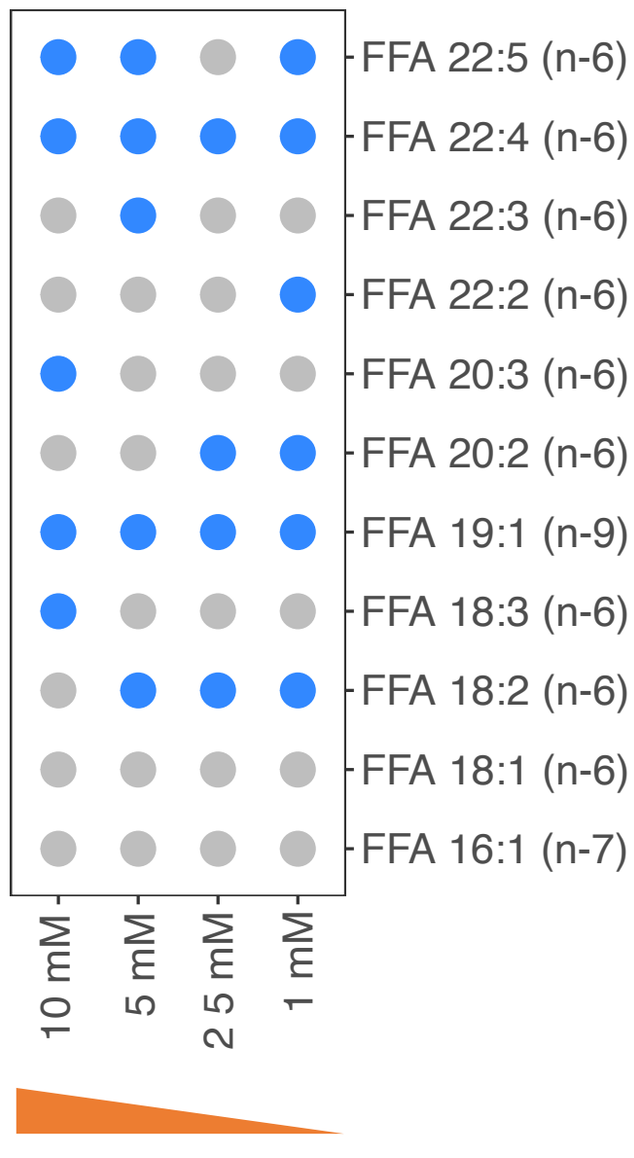

d